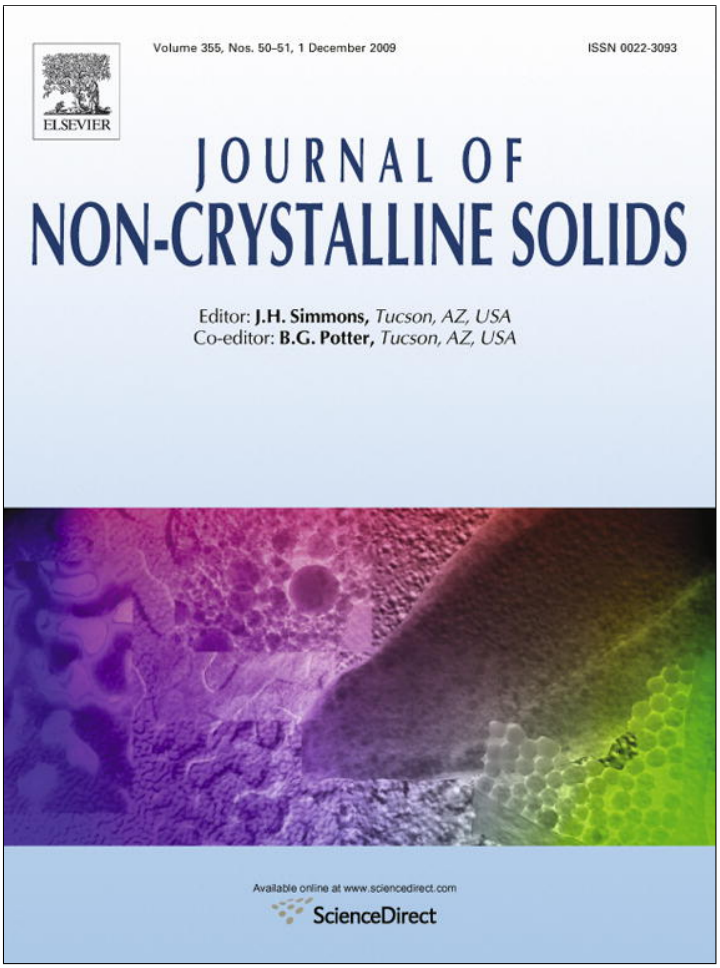

Journal of Non-Crystalline Solids 355 (2009) 2503–2507

Contents lists available at ScienceDirect

Journal of Non-Crystalline Solids

journal homepage: www.elsevier.com/locate/jnoncrysol

Stability and crystallization of $Fe_{81}B_{13}Si_4C_2$ amorphous alloy

D.M. Minić [a,*], D.G. Minić [b], A. Maričić [b]

[a] Faculty of Physical Chemistry, University of Belgrade, Belgrade, Serbia
[b] Technical Faculty Čačak, University in Kragujevac, Serbia

ARTICLE INFO

Article history:
Received 24 September 2008
Received in revised form 29 June 2009
Available online 26 September 2009

PACS:
61.43.-j
61.43.Dq
61.66.Fn

Keywords:
Amorphous metals
Metallic glasses
Alloys

ABSTRACT

The thermal stability and crystallization of the $Fe_{81}B_{13}Si_4C_2$ amorphous alloy were investigated in the temperature range of 300–1173 K. The correlation of the DSC and X-ray diffraction data with the measurements of electric and magnetic properties, which are very sensitive to structural changes, has shown a complex crystallization process involving at least two overlapping steps which appeared as one sharp slightly asymmetrical crystallization peak on the DSC curve. That could mean that the entire nucleation process did not take place during the early stage of the transformation and did not become negligible afterward. In this case, the crystallization rate is not defined by only the temperature but also depends on the previous thermal history of the alloy. This could be reason why the Johnson–Mehl–Avrami model usually used for the description of crystallization involving the stage of nucleation and the stage of growth of nuclei is not valid.

1. Introduction

Amorphous alloys, also known as metallic glasses, are non-crystalline materials usually obtained by the rapid cooling of melts having a disordered distribution of atoms in the cooled melt and an excellent combination of physical properties which are very important for their high technological applications [1]. Magnetic amorphous alloys based on Fe and Co possess outstanding soft-magnetic properties such as a high permeability, high saturation magnetization, low coercivity. These characteristics have enabled their use in modern technology and attracted great interest of many researches [2–5]. Amorphous alloys are metastable materials and during heating, these materials transform into a crystalline state. However, it is well known that the magnetic properties, as well as the electric properties, of these materials are structurally very sensitive and depend significantly on the manufacturing conditions of the alloys as well as their thermal history [6]. For technological applications, nano-structured soft-magnetic alloys obtained by partial crystallization from amorphous precursors [7,8] are very important. These nano-crystalline materials typically possess a microstructure of nano-crystals about 10 nm in size embedded in an amorphous matrix. This type of microstructure provides them with an efficient averaging of the magneto-crystalline anisotropy, enabling soft-magnetic properties superior to the crystalline alloys [9–11].

The crystallization of amorphous alloys upon heating can be performed in several ways. In calorimetric measurements two basic methods are in use, isothermal and non-isothermal. In both cases the differential scanning calorimetry technique (DSC) is the most common method to study the crystallization behavior of these materials. However, this method requires that the crystallization occurs with a relatively high heat of crystallization, and it is not useful when the crystallization occurs with a small heat transfer or at a slow rate. In such situations, the measurement of electrical resistivity or magnetic permeability has many advantages and gives more detailed information on the process of crystallization [12].

In our previous papers [13,14], non-isothermal research of the crystallization behavior and the kinetics and mechanism of crystallization of α-Fe from the $Fe_{81}B_{13}Si_4C_2$ amorphous ribbon produced by melt-spinning were reported. Based on the results of the DSC and X-ray diffraction analysis (XRD) and on the calculated crystallization parameters ($m = 3$; $s = 1$), we concluded that the primary crystallization of the α-Fe phase in an amorphous matrix occurs through the bulk nucleation and three-dimensional growth of nuclei growing at a constant rate [13]. It was established that the kinetic parameters of transformation did not change with the degree of crystallization α in the range of 0.1–0.7. Also, it was established that the primary crystallization of the α-Fe phase from an amorphous alloy cannot be described by the Johnson–Mehl–Avrami (JMA) model that is usually used for the description of crystallization involving a stage of nucleation as well as a stage of growth of nuclei. Rather it can be described by the Šesták–Berggren autocat-

* Corresponding author. Tel.: +381 11 3336 689; fax: +381 11 2187 133.
E-mail address: dminic@ffh.bg.ac.rs (D.M. Minić).

0022-3093/$ - see front matter © 2009 Elsevier B.V. All rights reserved.
doi:10.1016/j.jnoncrysol.2009.08.036

alytic model with the kinetic triplet $E_a = 349.4.0$ kJ mol^{-1}, ln $A = 50.76$ and $f(\alpha) = \alpha^{0.72}(1-\alpha)^{1.02}$ [14]. Therefore, for a detailed study of the process of crystallization, we have used electric and magnetic measurements since they are more sensitive to structural transformations.

2. Experimental details

The ribbon-shaped samples of the $Fe_{81}B_{13}Si_4C_2$ amorphous alloy were obtained using the standard procedure of rapid quenching of the melt on a rotating disc (melt-spinning). The resulting ribbon was 2 cm wide and 35 μm thick.

The crystallization process was investigated by the DSC technique in a nitrogen atmosphere using a SHIMADZU DSC-50 analyzer. In this case, samples weighing several milligrams were heated in the DSC cell from room temperature to 920 K in a stream of nitrogen with a flow rate of 20 mL min^{-1} and a heating rate of 5 K min^{-1}.

In order to investigate the structural transformations by the XRD technique, the samples of the amorphous alloy $Fe_{81}B_{13}Si_4C_2$ were annealed at the different temperatures (298–1173 K) in a stream of nitrogen during 30 min. The X-ray powder diffraction patterns for the as-prepared alloy, as well as for the samples that were annealed at different temperatures, were recorded on a Philips PW-1710 automated diffractometer using a Cu tube operated at 40 kV and 30 mA. The instrument was equipped with a diffracted beam curved graphite monochromator and Xe-filled proportional counter. For the routine characterization, the diffraction data were collected in the range of 2θ Bragg angles (4–100°Counting for 0.1 s). Silicon powder was used as an external standard for calibration of the diffractometer. All XRD measurements were done with solid ribbon-shaped samples at ambient temperature.

The electrical resistance of the ribbon was measured by the four-point method within a temperature range of 293–900 K in an argon atmosphere. Measurements of relative magnetic permeability were performed using a modified Maxwell method, based on the action of an inhomogeneous magnetic field on a magnetic sample. The magnetic force measurements were performed with a sensitivity of 10^{-6} N in an argon atmosphere. The sample of the alloy was mechanically coupled to a copper conductor, forming a $Cu–Fe_{81}B_{13}Si_4C_2$ thermocouple for the measurement of the thermo-electromotive force (TEMF). The thermocouple was placed into a specially designed furnace, while the other end of the sample was submerged into a mixture of water and ice. The TEMF produced by the thermocouple during the heating process was measured by a voltmeter of 10^{-5} V sensitivity.

3. Results and discussion

The amorphous state of the as-prepared alloy was confirmed by the X-ray diffraction method. The diffraction pattern for the as-prepared alloy, Fig. 1, has only a spread halo in the 2θ range of 40–50° and does not have appreciable diffraction peaks indicating an absence of the long-range crystalline order. This is characteristic for an amorphous structure which remained unchanged after annealing at 473 K. The size of the coherently scattering regions, calculated from the half-width of the observed halo by Scherrer's formula, is about 0.71 nm, pointing out the presence of highly disordered Fe clusters in an amorphous matrix.

The diffraction patterns of the annealed alloy, in the temperature range 473–733 K contain the same halo as the original sample as well as a sharp peak at $2\theta = 83.8°$ indicating the presence of a crystal phase as a consequence of the ordered Fe-clusters already present in the starting alloy. An increase of the annealed temperature results in a decrease of intensity of this peak and the appearance of a new sharp peak at $2\theta = 46.8°$. The height of the peak increases with an increase of the annealing temperature. This increased height, as well as a decrease of the half-width of the peak, indicates an increase of the crystallinity of an alloy. This shows that at temperatures above 770 K, primary crystallization occurs. Thoroughly studying of diffractograms by comparing the semi qualitative analysis of the annealed alloy, according to JPCDS card No. 06 6698, gives evidence of the presence of α-Fe crystallization in an annealed alloy. The disarranged ratio of peak intensities of the diffraction lines indicates a very disordered crystal structure whose disorder disappears with an increase of the annealing temperature according to the ratio of the heights of the diffraction peaks. In this case, 11.3 nm crystallites are formed.

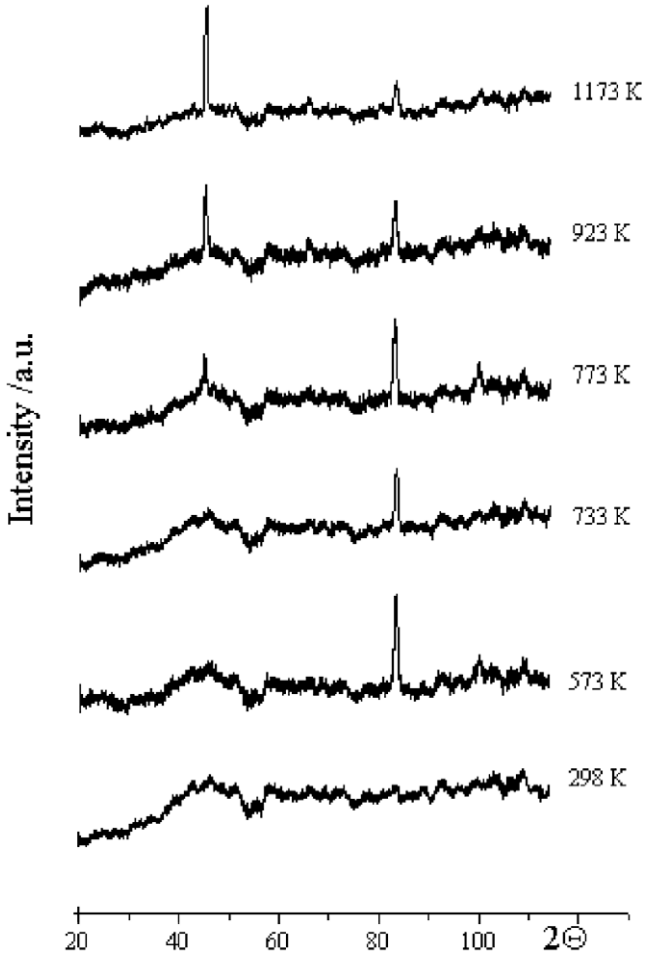

Fig. 1. XRD patterns for as-prepared and heated alloy.

The DSC curve (Fig. 2) involving the series of endo- and exo-peaks indicates a stepwise process of the alloy's structural stabil-

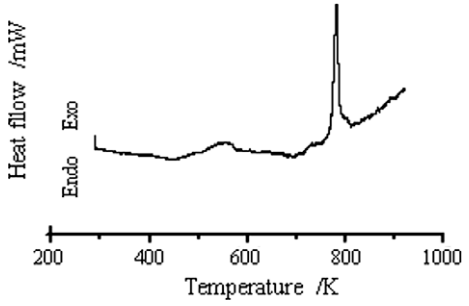

Fig. 2. DSC curve of alloy at heating rate 5 K/min.

ization in the temperature range of 470–810 K. A broad poorly formed exo-peak in the temperature range of 470–670 K corresponds to the structural relaxation processes in the as-prepared alloy. This peak is followed by an endothermic peak at 680 K corresponding to the Curie temperature T_c, an endothermic hump at about 780 K corresponding to the glass transition rather than the alloy, and a short super-cooled liquid region before a sharp exothermic crystallization peak, T_k, in the temperature range of 770–830 K. The observed single very sharp exothermic peak at 804 K could indicate a one-step crystallization process in the amorphous alloy.

The general equation for analysis of the conversion kinetics of partial crystallization of metallic alloys involving nucleation and growth in the solid phase was proposed by Avrami [15]:

$$\alpha(t) = 1 - \exp[-(kt)^n], \tag{1}$$

where $\alpha(t)$ is the degree of transformed volume, t is time, n is the kinetic exponent, and $k = k_0\exp(-E_a/RT)$. In the case of continuous heating when $E \gg RT$, the following relations were obtained:

$$\frac{\beta E}{k_p R T_p^2} = 1 \quad \text{and} \quad \frac{d\alpha}{dt} = 0.37 n k_p, \tag{2}$$

where β is the heating rate, E is the activation energy, T_p is the temperature of a peak, k_p is the rate constant at the peak and $d\alpha/dt$ is the crystallization rate at the peak.

By using the value of the activation energy [14], we found the values for the kinetic exponent and rate constants for the different rates of heating, Table 1.

The detailed study of the crystallization kinetics which was done by applying the Malek's procedure [16] to the DSC curves indicated the occurrence of a complex process of primary crystallization of the α-Fe phase in an amorphous matrix. Accordingly, the Johnson–Mehl–Avrami model usually used for the description of crystallization involving the stage of nucleation, as well as stage of growth of nuclei, was not applicable in this case [14].

The temperature dependence of the relative magnetic susceptibility of the as-prepared $Fe_{81}B_{13}Si_4C_2$ amorphous alloy during three cycles of heating to different temperatures is presented in Fig. 3. During the first and second heating, the decrease in the magnetic susceptibility in the temperature region from 590 K to 650 K is the result of getting closer to the Curie temperature of the amorphous alloy. After the first heating of the as-prepared alloy in the temperature region up to 660 K and cooling to room temperature, its magnetic susceptibility slightly increases. This increase of the magnetic susceptibility in the second heating was caused by the structural relaxation of an amorphous structure that developed during the first heating to 660 K. In this process, internal strains and the free volume are reduced in the starting material. These changes are accompanied by subtle inter-atomic movements, causing the changes in the electron structure. This leads to an increase in the number of electrons with unpaired spin in the direction of the outer magnetic field; this also leads to a decrease in the number of electrons spinning in the reverse direction and causes an increase in the magnetic susceptibility upon cooling. At the same time, strains and a decrease in the free volume during structural relaxation enable greater mobility of the walls of the magnetic

Table 1
Crystallization parameters of $Fe_{81}B_{13}Si_4C_2$ amorphous alloy $Fe_{81}B_{13}Si_4C_2$ amorphous alloy.

β (K min^{-1})	T_p (K)	k_p (min^{-1})	n
5	785.1 ± 0.1	0.31 ± 0.03	3.7 ± 0.1
10	793.2 ± 0.1	0.73 ± 0.03	4.1 ± 0.1
20	804.1 ± 0.1	1.27 ± 0.03	3.8 ± 0.1
30	811.4 ± 0.1	1.58 ± 0.03	3.6 ± 0.1

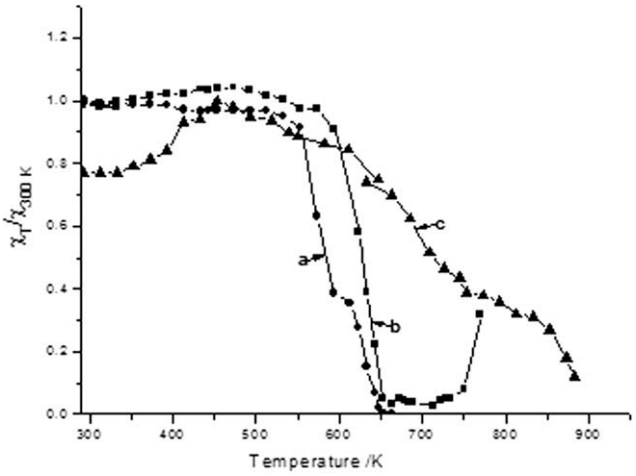

Fig. 3. Temperature dependence of relative magnetic susceptibility of as-prepared $Fe_{81}B_{13}Si_4C_2$ amorphous alloy during three cycles of heating up to different temperatures: (a) 690 K; (b) 770 K and (c) 900 K.

domains and this behavior further contributes to the increase in the magnetic susceptibility.

During the second heating and in the temperature region from 670 K to 740 K, the alloy loses its ferromagnetic properties. With further heating, the magnetic susceptibility starts to rise, and the alloy regains its ferromagnetic properties since the crystallization process starts at about 760 K. After the second heating to 760 K, the magnetic susceptibility decreases by 23% as compared to the value in its amorphous state and as compared to the value in its relaxed state after the first heating. During the third heating above the crystallization temperature, the alloy maintains its ferromagnetic features in the whole temperature region, whereas the maximum change in the magnetic susceptibility occurs at about 460 K as a consequence of further phase transformation of the crystallized alloy.

Fig. 4 shows the temperature dependence of the electrical resistivity of the amorphous alloy in the temperature range of 300–900 K. The electrical resistivity of the ordered (crystalline) alloy is lower than the disordered (amorphous) alloy of the same composition; therefore, the dependence clearly shows each structural stabilization step which causes the change in the ordering of the investigated material. The slow increase of electrical resistivity

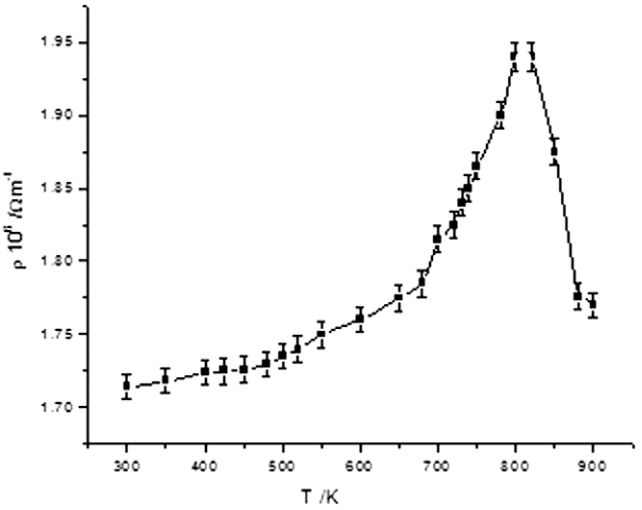

Fig. 4. Temperature dependence of the electrical resistivity of as-prepared $Fe_{81}B_{13}Si_4C_2$ amorphous alloy.

was caused by the structural relaxation processes in the temperature range of 470–650 K. This process is followed by an increase of electrical resistivity in the vicinity of Curie temperature T_c at 680 K according to the first maximum of the differential curve (Fig. 5) at which point the effect that the scattering of conductive electrons had on the magnons disappeared [17,18]. At that temperature, the amorphous alloy loses its ferromagnetic features, which is in excellent agreement with the results of the thermo-magnetic measurements (Fig. 3). The beginning of crystallization at about 790 K causes the sharp drop of electrical resistivity. The appearance of two clearly separated maxima, T_{k1} and T_{k2} (760 and 780 K, respectively) on the differential curve of electrical resistivity (Fig. 5), suggests that the process of the crystallization is a complex one and occurs in the two steps appearing as one overlapping peak in the DSC curves, Fig. 2.

The linear change of electrical resistivity with a rising temperature during the second heating shows that the process of crystallization was completed during the first heating to 900 K, Fig. 6.

The structural relaxation processes, as well as the crystallization process in the temperature interval of 300–950 K, were also investigated by measuring the thermo-electromotor force (TEMF) of a thermocouple made by joining a copper conductor and the amorphous alloy [19].

The temperature dependence of a thermo-electromotor force, Fig. 7, in agreement with the other results, shows three linear regions corresponding to the structural transformations of the alloy in a broad temperature range from 300 to 950 K. Different slopes of these linear dependences correspond to structural changes involving a structural relaxation, the loss of ferromagnetic properties, and the crystallization. The temperature coefficient TEMF is a function of the electron state density at the Fermi level:

$$\alpha = \frac{h^2}{2m_e}\left(\frac{3}{8\pi}\right)^{\frac{2}{3}}\left(N_{1(E_F)}^{\frac{2}{3}} - N_{2(E_F)}^{\frac{2}{3}}\right), \tag{3}$$

where h is Plank's constant, m_e is the mass of electrons, $N_{1(E_F)}$ is the electron state density in copper and $N_{2(E_F)}$ is the electron state density in the alloy.The electron state density in copper remained unchanged during its heating to 950 K, so the change of the temperature coefficient during the heating of the thermocouple was caused only by the change of the electron state density at the Fermi level in the alloy. Based on the slope of the temperature coefficient, the thermo-electromotor force of the first linear segment is α_1 = 9.4 μV/K, and the relative change in the electron state density of the alloy caused by the structural relaxation process was determined to be $\frac{\Delta N_1}{N} = 3.53\%$. The temperature coefficient of the thermo-electromotor force for the second linear segment is α_2 = 8.36 μV/K, and $\frac{\Delta N_2}{N} = 5.33\%$ was determined to be 5.33%. Finally, for the third linear segment, α_3 = 7.12 μV/K and $\frac{\Delta N_3}{N} = 7.81\%$ was 7.81%. The overall change in the electron state density at the Fermi level caused by the structural transformations during heating the alloy in temperature range 300–900 K is the sum of the three ΔN/N values or 16.67%.

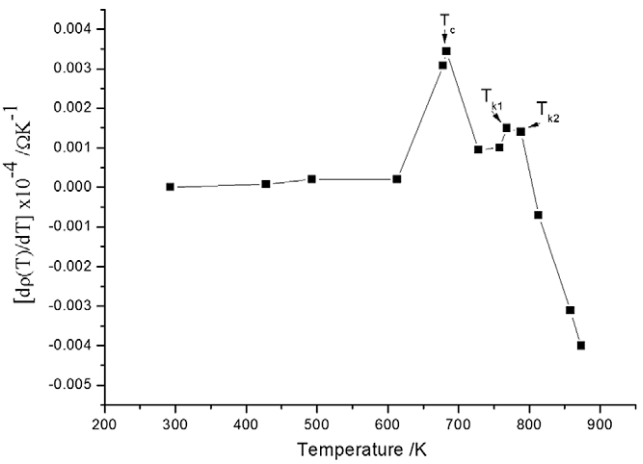

Fig. 5. First derivative of the electrical resistivity with the temperature of as-prepared $Fe_{81}B_{13}Si_4C_2$ amorphous alloy.

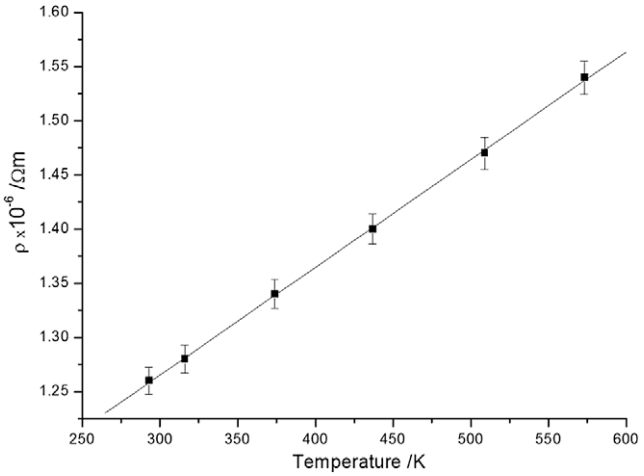

Fig. 6. Temperature dependence of the electrical resistivity of $Fe_{81}B_{13}Si_4C_2$ alloy during second heating.

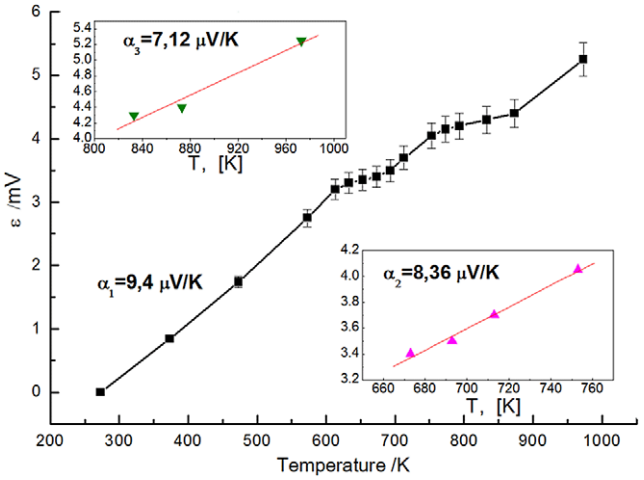

Fig. 7. Temperature dependence of thermo-electromotor force of thermocouple made by join a copper conductor and investigated alloy.

4. Conclusion

The crystallization kinetics of amorphous solids involving the steps of nucleation and the growth of nuclei is usually interpreted in terms of the Johnson–Mehl–Avrami (JMA) model. However, strictly speaking, this model is valid in isothermal conditions, and it can be rigorously applied to the transformations involving nucleation and growth only in a limited number of special cases in non-isothermal conditions. For the process of non-isothermal crystallization of the α-Fe phase in an amorphous $Fe_{81}B_{13}Si_4C_2$ alloy, a different analysis of DSC curves was used to show that the conditions for the validity of the JMA model are not fulfilled [14]. In this paper, a correlation of data of the DSC curves and X-ray diffraction techniques with the measurements of electric and magnetic properties was used since these techniques are very sensitive to structural changes. The results show why the conditions for the

validity of the JMA model are not fulfilled, namely that a complex crystallization process occurred and involved at least two overlapping steps which appeared as one sharp slightly asymmetrical crystallization peak on the DSC curve. That could mean that the entire nucleation process did not take place during the early stage of the transformation and became negligible afterward. In this case, the crystallization rate is not defined by only the temperature and depends on the previous thermal history of alloy.

Acknowledgements

The investigation was partially supported by the Ministry of Science and Environmental Protection of Serbia, under Project 142025.

References

[1] J.S. Blazquez, M. Millan, C.F. Conde, V. Franco, A. Conde, S. Lorenzo-Perez, J. Non-Cryst. Solids 354 (2009) 5135.
[2] I.C. Rho, C.S. Yoon, C.K. Kim, T.Y. Byun, K.S. Hong, Mater. Sci. Eng. B96 (2002) 48.
[3] T. Gloriant, S. Surinah, M.D. Baro, J. Non-Cryst. Solids 333 (2004) 48.
[4] M. Miglierini, J. Non-Cryst. Solids 354 (2009) 5093.
[5] M. Iqbal, J.I. Akhter, H.F. Zhang, Z.Q. Hu, J. Non-Cryst. Solids 354 (2009) 5363.
[6] M.G. Scott, in: F.E. Luborsky (Ed.), Amorphous Metallic Alloys, Butterworths, London, 1983, p. 144.
[7] M.A. Willard, V.G. Harris, JOM 3 (2002) 44.
[8] M.E. McHenry, M.A. Willard, D.E. Laughlin, Prog. Mater. Sci. 44 (1999) 291.
[9] H.F. Li, R.V. Ramanujan, Thin Solid Films 514 (2006) 316.
[10] R. Nicula, M. Stir, K. Ishizaki, J.M. Catala-Civera, S. Vaucher, Scripta Mater. 60 (2009) 120.
[11] N. Bayri, T. Izgi, H. Gencer, P. Sovak, M. Gunes, S. Atalay, J. Non-Cryst. Solids 355 (2009) 12.
[12] H.F. Li, R.V. Ramanujan, Mater. Sci. Eng. A375–377 (2004) 1087.
[13] D.M. Minić, A. Maričić, B. Adnađević, J. Alloys Compd. 473 (2009) 363.
[14] D.M. Minić, B. Adnađević, Thermochim. Acta 474 (2008) 41.
[15] M. Avrami, J. Chem. Phys. 15 (1979) 1103.
[16] J. Malek, Thermochim. Acta 355 (2000) 239.
[17] G. Bohnke, S.N. Kaul, W. Kettler, M. Rosenberg, Solid State Commun. 48 (9) (1983) 743.
[18] I. Balberg, J.S. Helman, Phys. Rev. B 18 (1) (1978) 303.
[19] L. Ribić-Zelenović, L. Rafailović, M. Spasojević, A. Maričić, Phys. B: Condens. Mat. 403 (2008) 2148.